Advancement of dengue virus NS1 protein detection by 3D-nanoassembly complex gold nanoparticles utilizing competitive sandwich aptamer on disposable electrode

Advancement of dengue virus NS1 protein detection by 3D-nanoassembly complex gold nanoparticles utilizing competitive sandwich aptamer on disposable electrode

Indra Memdi Khoris,[1] Fahmida Nasrin,[2] Ankan Dutta Chowdhury,[2,†] Enoch Y. Park[1,2,*]

[1]Department of Bioscience, Graduate School of Science and Technology, Shizuoka University, 836 Ohya Suruga-ku, Shizuoka 422-8529, Japan

[2]Research Institute of Green Science and Technology, Shizuoka University, 836 Ohya Suruga-ku, Shizuoka 422-8529, Japan

E-mail addresses:
Indra.memdi.khoris.17@shizuoka.ac.jp (IMK)
Fahmida.Nasrin.17@shizuoka.ac.jp (FM)
dc_ankan@yahoo.co.in (ADC)
park.enoch@shizuoka.ac.jp (EYP)

[*] Corresponding author at: Research Institute of Green Science and Technology, Shizuoka University, 836 Ohya, Suruga-ku, Shizuoka 422-8529, Japan.
E-mail address: park.enoch@shizuoka.ac.jp (E.Y. Park). Tel (Fax): +81-54-238-4887)
[†] Current address: Amity Institute of Nanotechnology, Amity University Kolkata, Major Arterial Road (South-East), AA II, West Bengal 700135, India

ABSTRACT

Signal amplification have been centralized in developing the biosensor for analyte detection with high reliability and narrow detection window. We proposed an aptasensor to provide a highly sensitive early-stage diagnostic platform of dengue virus NS1 protein (DENV-NS1) by dual-approach – colorimetric and electrochemical detection. This work utilized two different aptamers specific to DENV-NS1: One conjugated to gold nanoparticles (AuNPs), forming AuNPs-Apt_1 and its complementary sequence aptamer, forming AuNPs-Apt_2. The unbound Apt_1 of AuNPs-Apt_1 by DENV-NS1 were to hybridize to AuNPs-Apt_2 and induced a 3D-nanoassembled formation, resulting in DENV-NS1 concentration-dependent plasmonic color change. Occurrence of the hybridization of Apt_1 and Apt_2, the 3D-assembled hybridized aptamers of AuNPs was incubated with methylene blue (MB) solution, which intercalated a high number of MB molecules within the duplex structure of aptamers, and the complex was captured on the Apt_2-conjugated disposable gold electrode (DGE). The developed aptamer-based biosensor showed high sensitivity with colorimetric response down to 1.28 pg/mL and electrochemical approach down to 30 fg/mL of DENV-NS1 with good selectivity. This work showcases an advanced utilization of aptamer and its complementary anti-sense aptamer in signal amplification and nanocarrier for biosensing.

Keywords: gold nanoassembly, aptamer biosensor, colorimetric electrochemical, dengue virus NS1, redox nanocarrier

1. Introduction

In the last decades, dengue virus (DENV) infection has been a significant global health issue in tropical and sub-tropical countries worldwide [1]. This mosquito-borne viral infection disease is predicted to expand and continue to threaten more lives due to global warming, urbanization, and climate change [2]. Henceforward, tropical infectious diseases should have been an anticipated threat globally [3]. Currently, the available methods used for detecting DENV rely on cell culture [4], PCR [5] and ELISA assays [6]. These conventional diagnosis methods require sophisticated medical facilities as well as trained personnel which are not likely suitable for resource-limited settings [7]. Moreover, DENV is low in particle number during its earlier infection stage, which is a bottleneck for early detection [8, 9]. As an alternative, the non-structural protein 1 (NS1) protein of DENV (DENV-NS1) can be used because it holds clinical significance in the early phase [10, 11, 12].

Emerging aptamers-based biosensors (aptasensors) have attracted intensive attention in disease diagnostics, environmental monitoring, and surveillance of viral agents [13, 14, 15]. Presently, aptamers, a single-stranded oligonucleotide, have been progressively utilized in various fields due to their specific binding with their corresponding target with high affinity. Besides, aptamer possesses several advantages such as ease of chemical functionalization, high stability, and low cost with a little batch-to-batch variation [16]. In terms of simplicity, colorimetric-based aptasensors have been a preferable analytical methods that have been developed using nanozyme [17], localized surface plasmon resonance shift of plasmonic nanomaterial [18], and magnetic nanoparticles [18]. On the contrary, electrochemical-based aptasensor has recently dominated due to its higher signal-transducing properties [19, 20]. Unfortunately, the

71 developed methods only provided a single modality assay and may suffer from a lack of
72 signal amplification to establish a highly sensitive detection [21, 22].

73 Several pioneering works utilized liposomal nanoencapsulation to bring
74 multimodal sensing probes into the detection platform, combining optical and
75 electrochemical signal molecules [23, 24]. However, the existing nanocarrier has a
76 drawback of its encapsulation uniformity and prolonged protocol due to intermediate
77 steps to activate the sensing probes inside the nanostructure. Conversely, in the previously
78 reported works, utilizing the nanocarrier concept has opened a new approach in
79 developing biosensors to overcome the urgent demand on a wide dynamic range of
80 detection with more complementary information [15, 25]. Observing the need for more
81 straightforward detection with higher signal enhancement from the preceding works, a
82 feasible embodiment of intrinsic nanomaterial properties and utilization of nanocarrier
83 are demanded to escalate the performance of the aptasensor.

84 Gold nanoparticles (AuNPs) have been known to undergo a versatile and easy
85 conjugation of aptamer [26]. Herein, a dual-approach aptasensor was developed to
86 convey a more comprehensive dynamic range of individual detection platforms with a
87 combined feature, highly sensitive detection from an electrochemical signal, and a simple
88 readout from an improved visual change. Coupling of both concepts, nanocarrier and
89 sense-antisense competitive hybridization, the aptasensor was designed and developed to
90 exhibit a competitive colorimetric detection of DENV-NS1 aiming at early-diagnostic,
91 highly sensitive detection of DENV infection. Unlike a conventional single AuNPs-Apt
92 [27], the competitive complementary AuNPs-Apt induced a 3D-nanoassembly structure
93 of AuNPs which demonstrated a higher plasmonic color shift. Different from the general

electrochemical aptasensor using an individual conjugated redox probe [28], this finding exploited a nanocarrier-based electrochemical detection by incorporating methylene blue (MB) in the 3D-nanoassembly structure via MB-duplex aptamer interaction. The electrochemical signal from MB proved that it could enhance the detection signal down from picogram to femtogram level. Excitingly, the developed dual-approach aptasensor provided an advanced tool for a sensitive, simple, and label-free DENV-NS1 detection which holds great potential in an early-diagnostic biosensor to target infectious viruses that are very low concentration in the early infection stage.

2. Materials and methods

2.1. Materials, Instruments, and Preparation of Aptamer conjugated AuNPs (Apt_1- and Apt_2-conjugated AuNPs)

All the above methods are described in detail in **SI-1 Material and Instruments of** the Supplementary data.

2.2. Detection of dengue virus 2 NS1 protein in buffer and spike solution

2.2.1. Colorimetric detection

Dengue virus type 2 NS1 protein (DENV-NS1) was diluted to a series of concentrations. A 50 μL of the DENV-NS1 was mixed into PBS buffer containing $MgCl_2$ (1:1 v/v), and 100 μL of AuNPs-Apt_1 was added into the DENV-NS1 solution. The

115 mixture was incubated for the binding of Apt_1 to the DENV-NS1. The visual color and
116 absorbance were recorded. Next, the mixture was added with 50 μL AuNPs-Apt_2 solution.
117 The mixture was incubated to bind Apt_1 of the AuNPs-Apt_1 and Apt_2 of AuNPs-Apt_2. For
118 the analysis, A_{525} and A_{624} were recorded as the ratio parameter of the detection plot.

119 *2.2.2. Electrochemical detection*

120 The electrochemical detection was conducted on an Apt_2-modified disposable gold
121 electrode (DGE). Apt_2-modified DGE was prepared by incubating 10 μL of 1 μM thiol-
122 functionalized Apt_2. To translate the aptasensor into an electrochemical detection, the
123 AuNPs-Apt complex solution was added with 10 mM methylene blue (MB) solution (1:1
124 v/v). After incubation, the 15 μL mixture was drop-casted on the Apt_2-modified DGE.
125 Afterward, the solution was discarded, and the DGE was washed several times with PBS
126 buffer containing 1 mM $MgCl_2$. The working solution for the electrochemical detection
127 is PBS buffer with an additional 0.5 M NaCl. The differential pulse voltammetry (DPV)
128 analysis was conducted from – 0.5 V to + 0.2 V at a step potential of 25 mV/s and
129 modulation pulse and time of 50 mV and 50 ms, respectively. The obtained oxidation
130 peak of the DPV was used as the electrochemical signal.

131

132 **3. Results and discussion**

133

134 *3.1. Mechanism of the 3D-nanoassembled gold nanoparticles aptasensor*

135 The proposed aptasensor was designed based on the aptamer-conjugated AuNPs,
136 forming a competitive binding of AuNPs-Apt_1 to DENV-NS1 and its complementary

137 towards AuNPs-Apt_2. The detection mechanism was designed in two approaches;
138 colorimetric detection and electrochemical detection, as illustrated in **Scheme 1**. First,
139 AuNPs-Apt_1 were added into the detection sample and bound to the DENV-NS1 via
140 aptamer-DENV-NS1 affinity (**A**). In the presence of DENV-NS1, AuNPs-Apt_1 will bind
141 to the target DENV-NS1, forming AuNPs-Apt_1/DENV-NS1 (**B**). Next, the proposed
142 aptasensor was added the complementary AuNPs-Apt_2 (**C**) to bind to the unbound Apt_1
143 of AuNPs-Apt_1, forming AuNPs-Apt_1/AuNPs-Apt_2 3D-nanoassembled aggregation
144 (AuNPs-Apt complex) via Apt_1-Apt_2 hybridization (**D**). The induced aggregation
145 demonstrated the color change depending on the degree of aggregation, which would also
146 be dependent on the DENV-NS1 binding to the Apt_1 on the AuNPs-Apt_1 (AuNPs-Apt
147 complex-based detection).

148 <Scheme 1>

149 To utilize the 3D-nanoassembled AuNPs-Apt for electrochemical detection, the
150 methylene blue (MB) was added into the AuNPs-Apt complex and bound to the duplex
151 structure of the AuNPs-Apt complex by electrostatical intercalation [29]. Then, on the
152 surface of the DGE, the immobilized Apt_2 aptamer conjugated with the unbound Apt_1 of
153 AuNPs-Apt complex, forming the captured DGE/Apt_2/AuNPs-Apt_1(AuNPs-
154 Apt_2)(DENV-NS1). The MB amount is corresponding to the amount of the hybridized
155 complex of Apt_1 and Apt_2 within the 3D-nanoassembly, inversely proportional to the
156 DENV-NS1 concentration in the sample solution. As the free MB was washed out, the
157 oxidation peak in the DPV analysis indicates the amount of MB carried by the AuNPs-
158 Apt complex only.

159

160 *3.2. Characterization of the AuNPs-Apt$_1$, AuNPs-Apt$_2$, and 3D-nanoassembled AuNPs-*
161 *Apt complex*

162 Aptamers were conjugated to AuNPs by affinity binding as illustrated in **Fig. 1A**.
163 AuNPs-Apt$_1$ was prepared by conjugating biotin-functionalized Apt$_1$ with streptavidin-
164 functionalized AuNPs and AuNPs-Apt$_2$ was prepared by indirect method, conjugating via
165 Au-thiol coordination between AuNP with thiolated Apt$_2$. To confirm the conjugation of
166 the AuNPs-Apt, both functionalized AuNPs were characterized by absorbance, as shown
167 in **Fig. 1B.** After conjugation with Apt$_1$ and Apt$_2$, AuNPs retain their plasmonic properties
168 with peaks at 525 nm with no visible shoulder. In contrast to the single AuNPs-Apt, the
169 mixture demonstrated a change of the absorbance spectra with lower absorbance at 525
170 nm and immersed the secondary broad peak near 616 nm, indicating the aggregation
171 formation of AuNPs [30]. The image (inset of **Fig. 1B**) shows that AuNPs-Apt$_1$ and
172 AuNPs-Apt$_2$ have red-pinkish color, but the AuNPs-Apt$_1$/AuNPs-Apt$_2$ have a blue color,
173 fading in a longer incubation time.

174 <Figure 1>

175 The mixture of AuNPs-Apt$_1$ and AuNPs-Apt$_2$ was analyzed under transmission
176 electron microscopy (TEM) to understand the morphology of the aggregation of the
177 AuNP. As shown in **Fig 1C**, at first, AuNPs-Apt$_1$ was visibly well-dispersed with the size
178 of 20 nm. After 5 min, the interaction of AuNPs-Apt$_1$ and AuNPs-Apt$_2$ was demonstrated
179 by the initiation of the agglomeration of AuNPs. The aggregation of the AuNPs was
180 evitable in the presence of two AuNPs-Apt. In the conjugation of AuNP-Apt, the size of
181 two AuNPs were different; 20 nm for Apt whereas 5 nm for Apt$_2$. Due to the difference
182 of AuNPs' sizes, the time course TEM analysis was clearly visible in TEM images (**Fig.**

183 **1D**). In the initial time, single AuNPs-Apt_1 with a size of 20 nm was bound to the
184 individual of AuNPs-Apt_2 with a distinct size of 5 nm. In the longer incubation period,
185 the agglomeration of the combination of 20 nm and 5 nm of AuNPs was clearly visible.
186 Finally, a particular agglomeration degree was observed at a prolonged time where the
187 AuNPs-Apt_1 was shown to be surrounded and bounded by the AuNPs-Apt_2, bridging the
188 AuNPs via aptamer and its anti-sense aptamer [31, 32]. It is expected that the AuNPs-
189 Apt_1 and AuNPs-Apt_2 should be capable to bind each other in three-directional formation,
190 resulting the 3D-nanoassemble network of AuNPs.

191

192 *3.3. The colorimetric detection of DENV-NS1 using the plasmonic shift of AuNPs-*
193 *Apt_1/AuNPs-Apt_2 aptasensor*

194 The incubation time of AuNPs-Apt_1 were optimized to obtain the highest signal
195 of colorimetric change (**Fig. S1)**. As the incubation time was increased, the binding of
196 AuNPs-Apt_1 was elevated and reached the saturation at 20 min for binding DENV-NS1
197 (**Fig. S1A**) and the average of 5 min for the AuNPs-Apt_2 (**Fig. S1B**). The colorimetric
198 detection of the DENV-NS1 was conducted by a series of concentration of the target
199 analyte. The detection was done starting from the binding step of AuNPs-Apt_1 to DENV-
200 NS1 and continued to binding of AuNPs-Apt_2 to the free Apt_1 on AuNPs-Apt_1. As shown
201 in **Fig. 2A**, AuNPs-Apt_1 shows a single peak at 525 nm. With the increasing concentration
202 of DENV-NS1, the intensity of the shoulder peak at around 624 nm was also increasing.
203 In addition, the slight shift of the peak maxima was also observed increasing with the
204 DENV-NS1 concentration. Extending from the interaction of AuNPs-Apt_1-DENV-NS1,
205 AuNPs-Apt_2 was introduced to the mixture and intensified the change of the absorbance

206 spectrum. AuNPs-Apt_2 with no DENV-NS1 in the mixture (blank) has elevated shoulder
207 spectra with the lowest absorbance peak at 525 nm (**Fig. 2B**). These were different in
208 reverse to the AuNPs-Apt_1 after the DENV-NS1 addition. In the addition of AuNPs-Apt_2,
209 the agglomeration of the AuNPs-Apts was promoted since both aptamers would undergo
210 hybridization and lead the 3D-nanoassembly structure of AuNPs [33]. Opposite to the
211 previous trend the interaction of AuNPs-Apt_1 and DENV-NS1, the absorbance showed
212 lower shoulder absorbance with the increasing concentration of DENV-NS1. The
213 absorbance at 525 nm was higher than the control, indicating less aggregation of AuNPs
214 in the system, indicating that the conjugation between AuNPs-Apt_1 and DENV-NS1 was
215 less after-binding to the AuNPs-Apt_2. TEM analysis of the AuNPs-Apt_1/DENV-NS1 and
216 AuNPs-Apt_2 was shown in **Fig. S2**. Compared to the 3D-nanoassembly formation, the
217 presence of DENV-NS1 prior to the addition of AuNPs-Apt_2 leads to the smaller 3D-
218 nanoassembly formation, preventing to make aggregation of AuNP.

219 <Figure 2>

220 The ratio of A_{525}/A_{624} was plotted from the absorbance spectra as the function of
221 DENV-NS1 concentration. As shown in **Fig. 2C**, it showed an opposite correlation of the
222 absorbance change of AuNPs-Apt_1 between with the presence of the DENV-NS1,
223 showing positive function, and with the presence of both DENV-NS1 and AuNPs-Apt_2,
224 showing negative function. Based on the absorbance ratio, the direct detection of DENV-
225 NS1 using only AuNPs-Apt_1 showed a detection limit (LOD) of 124.83 pg/mL, based on
226 the 3 times standard deviation and blank signal according to the linearity of the aptasensor
227 [34]. However, the competitive detection by AuNPs-Apt_2 could demonstrate lower LOD,
228 down to 1.28 pg/mL DENV-NS1. Moreover, comparatively to the conventional single

229 aptamer-based aptasensor, AuNPs-Apt complex competitive formation resulted to
230 distinguishable color visual in the presence of the DENV-NS1 by naked eye observation
231 (**Fig. 2D**). Moreover, after 3.5 weeks of storage, the color change of the AuNPs-Apt_1 did
232 not show any observable change, but AuNPs-Apt_2 did undergo a minor decrease down to
233 a 2.5% change of absorbance (**Fig. S3A**). The complex AuNPs-Apt was still considerably
234 functional, with detection only down to 6.98% (**Fig. S3A**). The proposed aptasensor using
235 additional AuNPs-Apt_2 as the anti-sense to promote 3D-nanoassembly of the AuNPs, the
236 advancement strategy showcases an amplified ratiometric for detecting DENV-NS1.

237

238 *3.4. Electrochemical characterization of 3D-nanoassembled AuNPs-Apt as MB*
239 *nanocarrier*

240 In search of a more sensitive method, DGE was used as the biosensor platform
241 for easy and straightforward application. First, prior to the detection, the 3D-
242 nanoassembly AuNPs on the DGE was investigated whether it bound to the surface of
243 electrode. The electrochemical impedance spectroscopy (EIS) was conducted to
244 characterize the construction of the 3D-nanoassebled structure on the DGE. DGE showed
245 a typical Nyquist plot of Au-printed electrode (**Fig. 3A**). After the immobilization of Apt_2
246 on the DGE (DGE/Apt_2), the impedance of the electrode increased. Next, AuNPs-Apt_1
247 was captured on the DGE/Apt_2. The layer of AuNPs covers the surface of the DGE and
248 increases its electronic properties, indicated by lower impedance. In contrast, the
249 assembled of AuNPs-Apt_1/AuNPs-Apt_2 complex on the electrode resulted in higher
250 impedance.

251 The build-up network of the 3D-nanoassembly structure of AuNPs-Apt_1/AuNPs-
252 Apt_2 demonstrated different electronic properties than AuNPs-Apt_1. These indicate that a
253 single layer of AuNPs by AuNPs-Apt_1 had different electronic properties than a 3D-
254 nanoassembled structure of AuNPs on the DGE by the aptamer hybridization. In addition,
255 the presence of DENV-NS1 within the 3D-nanoassembled structure had a slightly higher
256 impedance due to the presence of larger biomolecules, such as DENV-NS1.

257 Further, cyclic voltammetry was applied on the DGE to understand the redox
258 behavior on the surface of the working electrode [35]. As shown in **Fig. 3B**, an observed
259 peak was in the run with a potential value of around 490 mV which showed a typical
260 reduction-oxidation profile of gold printed electrode [36]. The surface of the DGE was
261 profiled to understand the difference in the presence of AuNPs-Apt_1 and AuNPs-Apt_2. It
262 was observed that DGE/Apt_2/AuNPs-Apt_1 represented the single layer of AuNPs on the
263 DGE has a similar oxidation current like DGE/Apt. However, DGE/Apt_2/AuNPs-
264 Apt_1/AuNPs-Apt_2 resulted the 3D-nanoassembly AuNPs to isolate DGE's surface and
265 unexpectedly lowered the electrons current on the surface of the electrode and reduced
266 the oxidation peak in the cyclic voltammetry profile.

267 <Figure 3>

268 In this mechanism, AuNPs-Apt was acted as nanocarrier for the redox probe, MB
269 in the electrochemical detection. To investigate this, prior to the incubation of AuNPs-
270 Apt_1 and AuNPs-Apt_2 on the DGE/Apt_2, the AuNPs-Apt was incubated in MB solution
271 where the maximum amount of MB can be intercalated inside the aptamer. The loaded
272 amount of the MB was determined from the current value generated in DPV analysis [37]
273 (**Fig. 3C**). The standard oxidation peak of the MB was founded at –0.28 mV [38]. As

274 Apt_2 was bound to DGE directly, MB molecules chelated and showed higher DPV current
275 than unmodified DGE, increasing from – 3 μA to – 4.5 μA in intensity. This indicates
276 that the Apt_2 was conjugated successfully, and MB was chelated on the capture probe.
277 This is determined here as the noise/background signal in the electrochemical detection.
278 Further, in the presence of captured AuNPs-Apt on the surface of DGE/Apt_2, the DPV
279 analysis indicated a high signal of MB in DGE/Apt_2/AuNPs-Apt_1 and DGE/Apt_2/AuNPs-
280 Apt_1/AuNPs-Apt_2 with the current intensity of – 16 μA and – 27 μA, respectively. Based
281 on the preliminary study from the MB within the AuNPs-Apt, the signal-to-noise ratio
282 was calculated around 3-fold for AuNPs-Apt_1-based nano-assembly and 6-fold for
283 AuNPs-Apt_1/AuNPs-Apt_2-based 3D-nanoassembly structure. These signals were
284 demonstrated to be 2.4% in coefficient of variance on 10 independent DGEs, showing an
285 appropriate signal transducer for the electrochemical aptasensor (**Fig. S4**). In a control
286 experiment of AuNPs-Apt nanoassembly in absence of MB, it was observed an ignorable
287 hump of oxidation current between potential value of – 250 mV to – 450 mV (**Fig. 3D**),
288 like the bare DGE's potential value with the current around – 2.5 μA. It is clearly shown
289 that the MB as a redox probe is the only responsible source of current in this
290 electrochemical detection.

291

292 *3.5. The electrochemical detection of DENV-NS1 using the AuNPs-Apt_1/AuNPs-Apt_2*
293 *aptasensor*

294 The electrochemical detection of the DENV-NS1 was carried out after incubating
295 the AuNPs-Apt complex/DENV-NS1 in MB solution. MB's oxidation peak was observed
296 at potential around – 250 mV shown in **Fig. 4A**. As the concentration of the DENV-NS1

297 increased, the differential current, known as I delta in DPV analysis (ΔI), increased.
298 Moreover, it was observed the dominant peak from – 250 mV was coupled to peak at
299 potential around –320 mV which represents the MB contribution on DGE. A higher
300 concentration of the DENV-NS1 was resulted to lower the oxidation peak in the DPV,
301 while increasing the I delta value from negative value to less negative value. In absence
302 of target, the conjugated aptamers-AuNPs contain maximum number of MB, resulting
303 strong peak at –250 mV. After gradual increase of DENV-NS1, the peak of MB was
304 decreasing gradually and shifted towards –320 mV, which is the signal of DGE, in
305 presence of MB. In case of high concentration of target DENV-NS1, all apt_1 are
306 completely blocked and there is no space for MB loading on the electrode surface. As a
307 result, the peak intensity in DPV is almost insignificant like the bare electrode without
308 MB. The change of I delta ($\Delta I - \Delta I_{blank}$) at –250 mV was plotted as the function of the
309 concentration of DENV-NS1 (**Fig. 4B**). The proposed aptasensor demonstrated a linear
310 detection of 1 pg/mL – 1 ng/mL DENV-NS1 with $R^2 = 0.992$. However, over 1 ng/mL
311 DENV-NS1 concentration, it showed to be saturated with a higher cluttering signal
312 observed in a higher-level concentration, where the detection limit was calculated 30
313 fg/mL, which is 100-times lower than the colorimetric detection. This result emphasizes
314 the advantage of the 3D-nanoassembly structure of AuNPs-Apt as a nanocarrier in the
315 electrochemical detection. A comparative study on previously published works were
316 summarized in **Table S1** [39–41], showing that the detection limit of the proposed
317 aptasensor was superior in terms of detection limit and dynamic range.

318 <Figure 4>

319 The selectivity of this dual detection was assayed in 100 pg/mL different non-
320 target analytes, including norovirus-like particles (NoV-LPs), inactivated Influenza virus
321 A/H1N1 and A/H3N2. As shown in **Fig. 4C**, there is a slight change of signal ranging
322 from 98% – 102% based on the blank solution in either of the non-target analytes.
323 However, in the presence of target analytes of 100 pg/mL DENV-NS1, the signal was
324 changed to 80% for colorimetric detection and 40% for electrochemical detection. It
325 showed that even in a picogram concentration of target, electrochemical detection could
326 demonstrate a good specificity towards DENV-NS1. Further, in the spike solution of 2%
327 human serum, the proposed aptasensor could perform well for DENV-NS1 detection with
328 a relative standard deviation (RSD) ranging from 6.1% to 10.2% (**Table S2**), which was
329 acceptable as the detection variance. However, despite a considerably low RSD value,
330 the developed aptasensor still showed an interfering effect in serum, probably coming
331 from the buffer constituents and the lysate-derived proteins [42]. It was recommendable
332 to minimize the interferences by employing up to 50-fold dilution in the biological
333 complex matrix virus detection as for a pre-treatment and pre-dilution in the practical use.

334

335 **4. Conclusions**

336 This work reported a dual-detection aptasensor utilizing aptamers-conjugated
337 AuNPs to amplify the signal by 3D-nanoassembled formation. By introducing hybridized
338 duplex aptamer as a bridge of plasmonic aggregation, the 3D-nanoassembled formation
339 intensified the visual color change and provided a nanocarrier function for
340 electrochemical detection. The DENV-NS1 was detected by the disruption of the duplex
341 formation which would prevent the plasmonic color change and redox nanocarrier's

342 moiety of the 3D-nanoassembled AuNPs. It showcased a LOD down to 1.28 pg/mL in
343 colorimetric and 30 fg/mL in electrochemical approaches. Considering the mechanism of
344 the signal amplification, the developed strategy aimed to deliver an elevated concept of
345 the general approach in aptamer-based detection and establishing an early-diagnostic
346 method in low virus concentration or low available biomarker.

347

348 **CRediT authorship contribution statement**

349 **Indra Memdi Khoris:** Conceptualization, Methodology, Writing – original draft.
350 **Fahmida Nasrin:** Methodology, Writing – review & editing. **Ankan Dutta**
351 **Chowdhury:** Data interpretation, data analysis, Writing – review & editing. **Enoch Y.**
352 **Park:** Conceptualization, Writing – review & editing, Supervision.

353

354 **Declaration of competing interest**

355 The authors declare that they have no competing financial interest or personal
356 relationships that could have appeared to influence the work reported in this paper.

357

358 **Acknowledgment**

359 IMK sincerely thank the Japan Society for the Promotion of Science (JSPS) for
360 a research fellowship-DC (20J22358). This work was partially supported by the Fund
361 for the Promotion of Joint International Research, Fostering Joint International Research
362 B (Grant No. 20KK0115) and the Japan Agency for Medical Research and
363 Development (20hm0102080h0001).

Appendix A. Supplementary data

Comparison of dengue virus NS1 detection with previously published works, detection of dengue virus NS1 spike samples in human serum, optimization of the aptasensor, and TEM of dengue virus NS1 conjugated to AuNPs-Apt nanoassembly. Supplementary data to this article can be found, in the online version, at doi:https://doi:

References

[1] N. Yanagisawa, K. Wada, J.D. Spengler, R. Sanchez-Pina, Health preparedness plan for dengue detection during the 2020 summer Olympic and Paralympic games in Tokyo, PLoS Negl.Trop. Dis., 12 (2018) e0006755.

[2] F.J. Colón-González, M.O. Sewe, A.M. Tompkins, H. Sjödin, A. Casallas, J. Rocklöv, et al., Projecting the risk of mosquito-borne diseases in a warmer and more populated world: a multi-model, multi-scenario intercomparison modelling study, The Lancet Planetary Health, 5 (2021) e404–e414.

[3] M.A. Kabir, H. Zilouchian, M.A. Younas, W. Asghar, Dengue Detection: Advances in Diagnostic Tools from Conventional Technology to Point of Care, Biosensors, 11 (2021) 206.

[4] E. Iswardy, T.-C. Tsai, I.-F. Cheng, T.-C. Ho, G.C. Perng, H.-C. Chang, A bead-based immunofluorescence-assay on a microfluidic dielectrophoresis platform for rapid dengue virus detection, Biosens. Bioelectron., 95 (2017) 174–180.

[5] P.R. Abraham, R. Bharathy, P. Kumar, A. Kumar, Dengue NS1 antigen kit shows high sensitivity for detection of recombinant dengue virus-2 NS1 antigen spiked with Aedes aegypti mosquitoes, Sci. Rep., 11 (2021) 23699.

[6] A. Vázquez-Guardado, F. Mehta, B. Jimenez, A. Biswas, K. Ray, A. Baksh, et al., DNA-Modified Plasmonic Sensor for the Direct Detection of Virus Biomarkers from the Blood, Nano Lett., 21 (2021) 7505–7511.

[7] R. Eivazzadeh-Keihan, P. Pashazadeh-Panahi, T. Mahmoudi, K.K. Chenab, B. Baradaran, M. Hashemzaei, et al., Dengue virus: a review on advances in detection and trends–from conventional methods to novel biosensors, Microchim. Acta, 186 (2019) **3**249.

[8] S.-C. Lai, Y.-Y. Huang, P.-Y. Shu, S.-F. Chang, P.-S. Hsieh, J.-J. Wey, et al., Development of an enzyme-linked immunosorbent assay for rapid detection of dengue virus (DENV) NS1 and differentiation of DENV serotypes during early infection, J. Clin. Microbiol., 57 (2019) e00221–00219.

[9] O. Parkash, M.A. Abdullah, C.Y. Yean, S.D. Sekaran, R.H. Shueb, Development and Evaluation of an Electrochemical Biosensor for Detection of Dengue-Specific IgM Antibody in Serum Samples, Diagnostics, 11 (2021) 33.
[10] A. Dhal, T. Kalyani, S. Ghorai, N.K. Sahu, S.K. Jana, Recent development of electrochemical immunosensor for the diagnosis of dengue virus NSI protein: A review, Sensors International, (2020) 100030.
[11] D. Wasik, A. Mulchandani, M.V. Yates, Point-of-use nanobiosensor for detection of dengue virus NS1 antigen in adult Aedes aegypti: a potential tool for improved dengue surveillance, Anal. Chem., 90 (2018) 679–684.
[12] P.P.A. Suthanthiraraj, A.K. Sen, Localized surface plasmon resonance (LSPR) biosensor based on thermally annealed silver nanostructures with on-chip blood-plasma separation for the detection of dengue non-structural protein NS1 antigen, Biosens. Bioelectron., 132 (2019) 38–46.
[13] X. Liu, H. Zhang, S. Qin, Q. Wang, X. Yang, K. Wang, Optical fiber amplifier for quantitative and sensitive point-of-care testing of myoglobin and miRNA-141, Biosens. Bioelectron., 129 (2019) 87–92.
[14] Z. Zhang, L. Dong, Q. Zhu, Rational engineering of synergically stabilized aptamer-cDNA duplex probes for strand displacement based electrochemical sensors, Electrochim. Acta, 282 (2018) 588–594.
[15] X. Zhang, H. Zhi, M. Zhu, F. Wang, H. Meng, L. Feng, Electrochemical/visual dual-readout aptasensor for Ochratoxin A detection integrated into a miniaturized paper-based analytical device, Biosens. Bioelectron., 180 (2021) 113146.
[16] T.T.-Q. Nguyen, E.R. Kim, M.B. Gu, A new cognate aptamer pair-based sandwich-type electrochemical biosensor for sensitive detection of Staphylococcus aureus, Biosens. Bioelectron., 198 (2022) 113835.
[17] P. Weerathunge, R. Ramanathan, V.A. Torok, K. Hodgson, Y. Xu, R. Goodacre, et al., Ultrasensitive colorimetric detection of murine norovirus using NanoZyme aptasensor, Anal. Chem., 91 (2019) 3270–3276.
[18] L. Xu, R. Chopdat, D. Li, K.T. Al-Jamal, Development of a simple, sensitive and selective colorimetric aptasensor for the detection of cancer-derived exosomes, Biosens. Bioelectron., 169 (2020) 112576.
[19] A. Idili, C. Parolo, R. Alvarez-Diduk, A. Merkoçi, Rapid and efficient detection of the SARS-CoV-2 spike protein using an electrochemical aptamer-based sensor, ACS Sens., 6 (2021) 3093–3101.
[20] S. Sheibani, L. Capua, S. Kamaei, S.S.A. Akbari, J. Zhang, H. Guerin, et al., Extended gate field-effect-transistor for sensing cortisol stress hormone, Commun. Mater., 2 (2021) 10.
[21] K. Takemura, A.B. Ganganboina, I.M. Khoris, A.D. Chowdhury, E.Y. Park, Plasmon Nanocomposite-Enhanced Optical and Electrochemical Signals for Sensitive Virus Detection, ACS Sens., 6 (2021) 2605–2612.
[22] A.B. Ganganboina, A.D. Chowdhury, I.M. Khoris, R.-a. Doong, T.-C. Li, T. Hara, et al., Hollow magnetic-fluorescent nanoparticles for dual-modality virus detection, Biosens. Bioelectron., 170 (2020) 112680.
[23] A.B. Ganganboina, A.D. Chowdhury, I.M. Khoris, F. Nasrin, K. Takemura, T. Hara, et al., Dual modality sensor using liposome-based signal amplification technique for ultrasensitive norovirus detection, Biosens. Bioelectron., 157 (2020) 112169.

[24] F. Nasrin, A.D. Chowdhury, A.B. Ganganboina, O.J. Achadu, F. Hossain, M. Yamazaki, et al., Fluorescent and electrochemical dual-mode detection of Chikungunya virus E1 protein using fluorophore-embedded and redox probe-encapsulated liposomes, Microchim. Acta, 187 (2020) 674.
[25] I.M. Khoris, A.B. Ganganboina, E.Y. Park, Self-Assembled Chromogenic Polymeric Nanoparticle-Laden Nanocarrier as a Signal Carrier for Derivative Binary Responsive Virus Detection, ACS Appl. Mater. Interfaces, 13 (2021) 36868–36879.
[26] R. Gupta, A. Kumar, S. Kumar, A.K. Pinnaka, N.K. Singhal, Naked eye colorimetric detection of Escherichia coli using aptamer conjugated graphene oxide enclosed Gold nanoparticles, Sens. Actuators, B, 329 (2021) 129100.
[27] V. Morya, S. Walia, B.B. Mandal, C. Ghoroi, D. Bhatia, Functional DNA based hydrogels: development, properties and biological applications, ACS Biomater. Sci. Eng., 6 (2020) 6021–6035.
[28] C. Wang, Q. Zhao, A reagentless electrochemical sensor for aflatoxin B1 with sensitive signal-on responses using aptamer with methylene blue label at specific internal thymine, Biosens. Bioelectron., 167 (2020) 112478.
[29] E. Farjami, L. Clima, K.V. Gothelf, E.E. Ferapontova, DNA interactions with a methylene blue redox indicator depend on the DNA length and are sequence specific, Analyst, 135 (2010) 1443–1448.
[30] A. Baeissa, N. Dave, B.D. Smith, J. Liu, DNA-functionalized monolithic hydrogels and gold nanoparticles for colorimetric DNA detection, ACS Appl. Mater. Interfaces, 2 (2010) 3594–3600.
[31] M.Q. He, S. Chen, K. Yao, K. Wang, Y.L. Yu, J.H. Wang, Oriented assembly of gold nanoparticles with freezing‐driven surface DNA manipulation and its application in SERS‐based MicroRNA assay, Small Methods, 3 (2019) 1900017.
[32] M. Luo, M. Xuan, S. Huo, J. Fan, G. Chakraborty, Y. Wang, et al., Four‐Dimensional Deoxyribonucleic Acid‐Gold Nanoparticle Assemblies, Angew. Chem. Int. Ed., 59 (2020) 17250–17255.
[33] M.-Q. He, S. Chen, K. Yao, J. Meng, K. Wang, Y.-L. Yu, et al., Precisely Tuning LSPR Property via "Peptide-Encoded" Morphological Evolution of Gold Nanorods for Quantitative Visualization of Enzyme Activity, Anal. Chem., 92 (2019) 1395–1401.
[34] I.M. Khoris, A.B. Ganganboina, T. Suzuki, E.Y. Park, Self-assembled chromogen-loaded polymeric cocoon for respiratory virus detection, Nanoscale, 13 (2021) 388–396.
[35] A. Dutta Chowdhury, A.B. Ganganboina, F. Nasrin, K. Takemura, R.-a. Doong, D.I.S. Utomo, et al., Femtomolar detection of dengue virus DNA with serotype identification ability, Anal. Chem., 90 (2018) 12464–12474.
[36] V. Rodovalho, G. Araujo, E. Vaz, C. Ueira-Vieira, L. Goulart, J. Madurro, et al., Peptide-based electrochemical biosensor for juvenile idiopathic arthritis detection, Biosens. Bioelectron., 100 (2018) 577–582.
[37] S. Khezrian, A. Salimi, H. Teymourian, R. Hallaj, Label-free electrochemical IgE aptasensor based on covalent attachment of aptamer onto multiwalled carbon nanotubes/ionic liquid/chitosan nanocomposite modified electrode, Biosens. Bioelectron., 43 (2013) 218–225.
[38] S.M. Taghdisi, N.M. Danesh, M.A. Nameghi, M. Ramezani, M. Alibolandi, M. Hassanzadeh-Khayat, et al., A novel electrochemical aptasensor based on

492 nontarget-induced high accumulation of methylene blue on the surface of electrode
493 for sensing of α-synuclein oligomer, Biosens. Bioelectron., 123 (2019) 14–18.
494 [39] A. Santos, P.R. Bueno, J.J. Davis, A dual marker label free electrochemical assay
495 for Flavivirus dengue diagnosis, Biosens. Bioelectron., 100 (2018) 519–525.
496 [40] B.B. Junior, M.R. Batistuti, A.S. Pereira, E.M. de Sousa Russo, M. Mulato,
497 Electrochemical aptasensor for NS1 detection: Towards a fast dengue biosensor,
498 Talanta, 233 (2021) 122527.
499 [41] M.H. Nawaz, A. Hayat, G. Catanante, U. Latif, J.L. Marty, Development of a
500 portable and disposable NS1 based electrochemical immunosensor for early
501 diagnosis of dengue virus, Anal. Chim. Acta, 1026 (2018) 1–7.
502 [42] J. Tate, G. Ward, Interferences in immunoassay, The clinical biochemist reviews,
503 25 (2004) 105.
504

505

506 **Figure Caption**

507 **Scheme 1.** Proposed 3D-nanoassembled gold nanoparticles-based aptasensor designed
508 for colorimetric detection and electrochemical detection. **(A)** and **(C)** indicate AuNPs-
509 Apt_1 and AuNPs-Apt_2 as the detection probes; **(B)** shows DENV-NS1 binding to AuNPs-
510 Apt_1 and **(D)** shows 3D-nanoassembly of AuNPs; **(E)** indicates electrochemical detection
511 step and **(F)** shows the 3D-nanoassembled AuNPs captured on the Apt_2-modified DGE.

512 **Fig. 1.** Characterization of 3D-nanoasembly aggregation of AuNPs-Apt_1 and AuNPs-
513 Apt_2. (**A**) The illustration of the preparation of AuNPs-Apt_1 and AuNPs-Apt_2; (**B**)
514 Absorbance and visual images of the AuNPs-Apt_1 (1), AuNPs-Apt_2 (2) and AuNPs-
515 Apt_1/AuNPs-Apt_2 (3); TEM images of time-dependent nanoassembled formation of (**C**)
516 AuNPs-Apt_1 (20)/AuNPs-Apt_2 (20), and (**D**) AuNPs-Apt_1 (20)/AuNPs-Apt_2 (5). The
517 scale bars of the images are represented on each image.

518 **Fig. 2.** The colorimetric detection of DENV-NS1 using the proposed aptasensor. The
519 absorbance spectra of the AuNPs-Apt_1 after the addition of DENV-NS1 (**A**) and the
520 addition of DENV-NS1 and AuNPs-Apt_1 (**B**); (**C**) indicates the comparative plot of
521 DENV-NS1 concentration vs. ratiometric of A_{525} and A_{624} (the error bars indicate the
522 standard errors based on three measurements); (**D**) the visual image represents the color
523 change in determining the concentration of DENV-NS1 by the proposed aptasensor.

524 **Fig. 3.** 3D-nanoassembly AuNPs as the nanocarrier for electrochemical performance on
525 a disposable gold electrode (DGE). (**A**) Electrochemical Impedance Spectroscopy (EIS)
526 and (**B**) Cyclic voltammetry (CV) of the captured AuNPs-Apt_1/AuNPs-Apt_2 on Apt_2-

527 functionalized DGE with scan rate of 75 mV/s; Electrochemical performance of captured
528 3D-nanoassembly AuNPs-Apt_1/AuNPs-Apt_2 with MB (**C**) and without (**D**).

529 **Fig. 4.** The electrochemical detection of DENV-NS1 using the proposed aptasensor on
530 Apt_2-immobilized Disposable Gold Electrode (DGE). (**A**) DPV analysis of the aptasensor
531 in response in the DENV-NS1 detection; (**B**) semi-*log* plot of change of differential
532 current (ΔI) vs. concentration of DENV-NS1; (**C**) The selectivity test of proposed
533 aptasensor using colorimetric detection and electrochemical detection. The error bars in
534 **B** and **C** denote the standard errors from three measurements.

535

536 **Scheme 1**

537

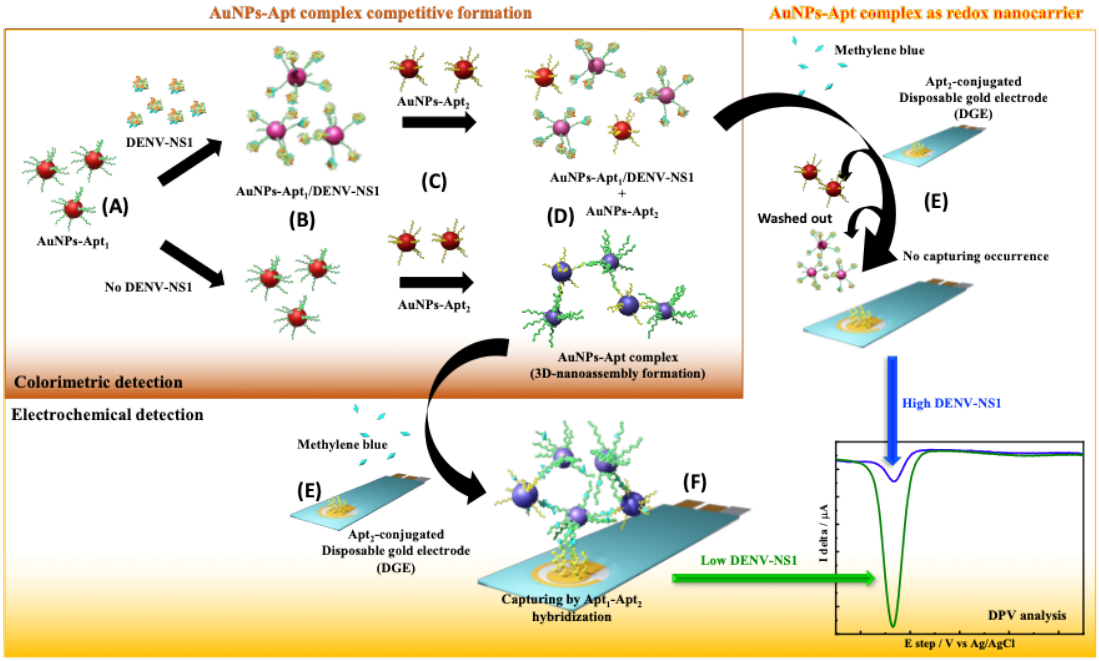

538

539

Fig. 1

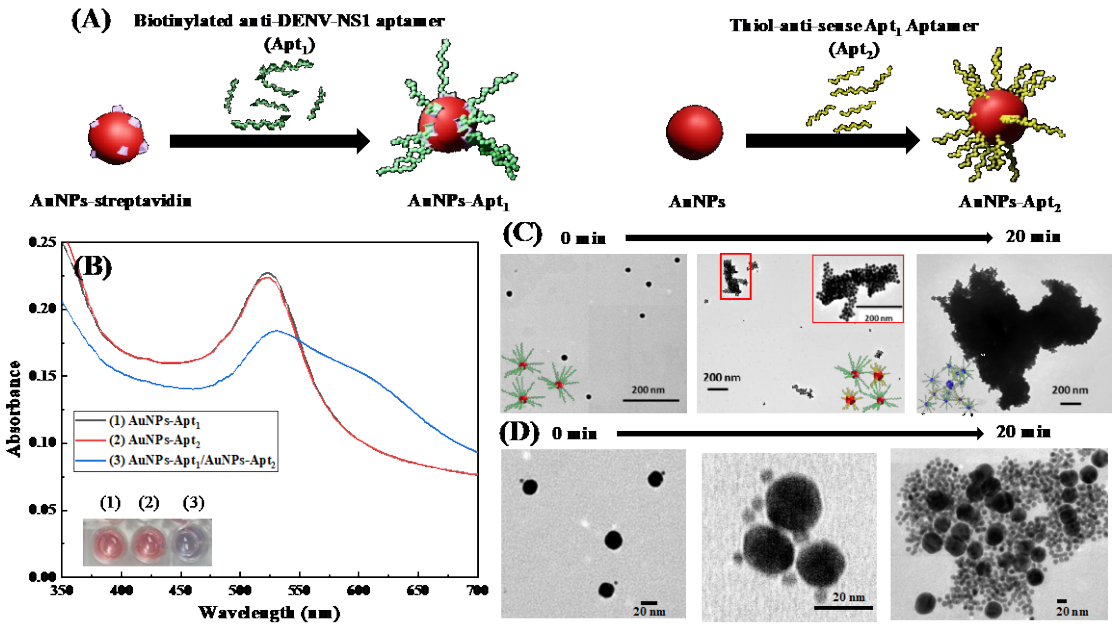
(A)
Biotinylated anti-DENV-NS1 aptamer
(Apt1)
AuNPs-streptavidin
AuNPs-Apt1
Thiol-anti-sense Apt1 Aptamer
(Apt2)
AuNPs
AuNPs-Apt2
(B)
Absorbance
Wavelength (nm)
(1) AuNPs-Apt1
(2) AuNPs-Apt2
(3) AuNPs-Apt1/AuNPs-Apt2
(1) (2) (3)
(C) 0 min
20 min
200 nm
(D) 0 min
20 min
20 nm

Fig. 2

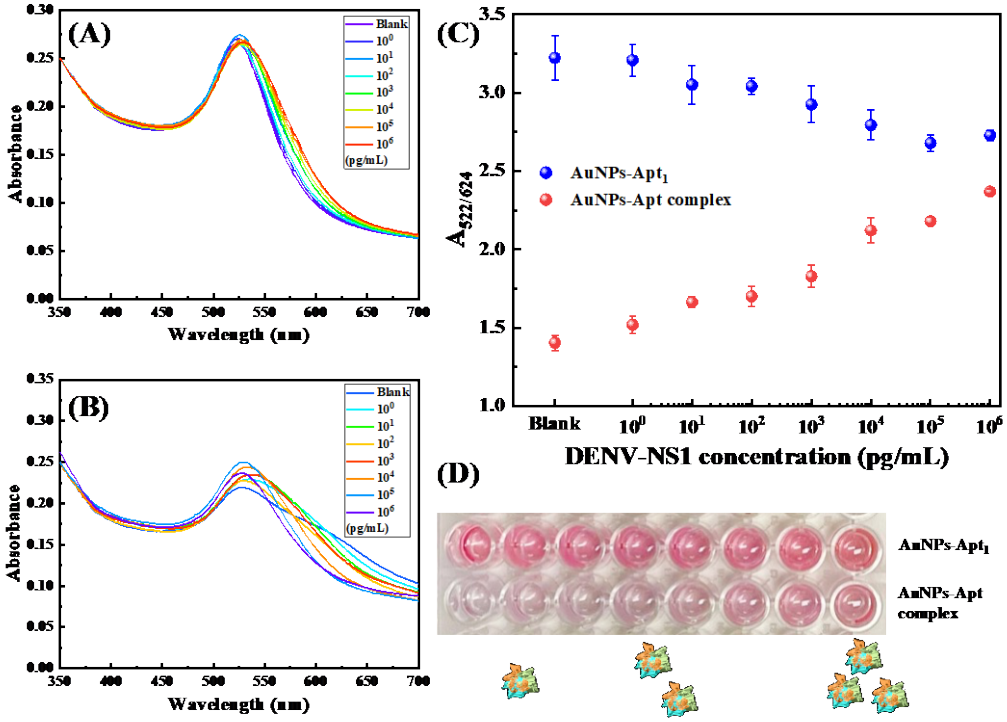
(A)
Absorbance
Wavelength (nm)
Blank
10^0
10^1
10^2
10^3
10^4
10^5
10^6
(pg/mL)
(B)
Absorbance
Wavelength (nm)
(C)
$A_{522/624}$
AuNPs-Apt$_1$
AuNPs-Apt complex
DENV-NS1 concentration (pg/mL)
(D)
AuNPs-Apt$_1$
AuNPs-Apt complex

Fig. 3

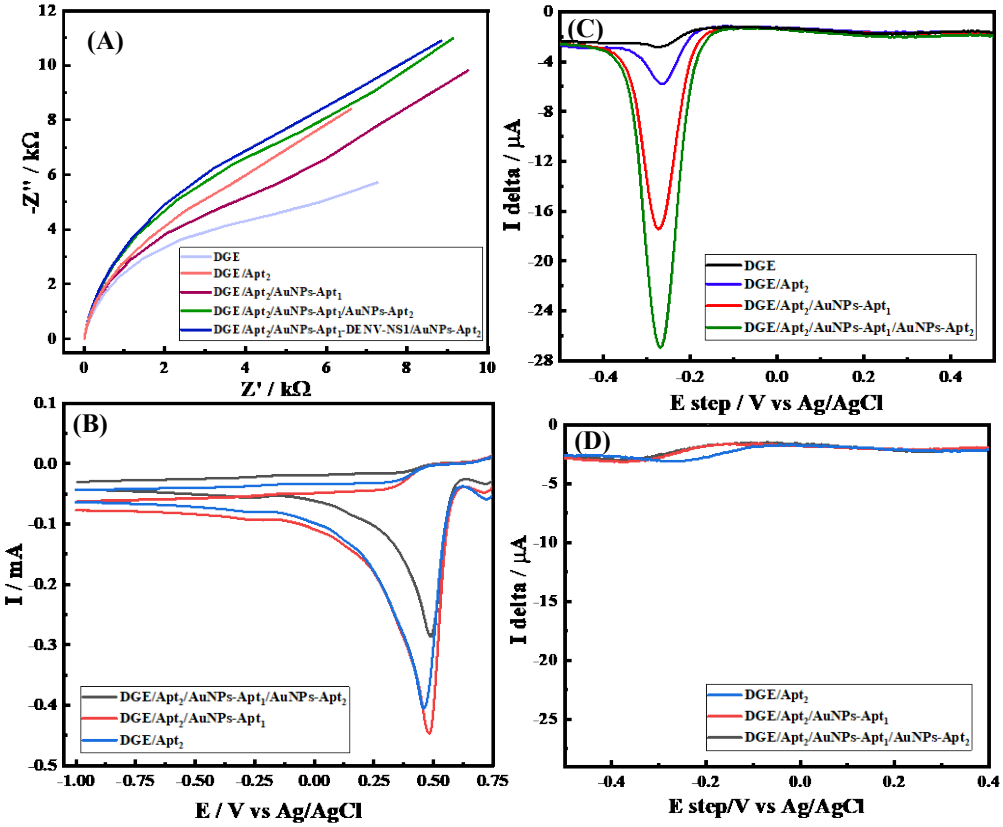
(A)
-Z'' / kΩ
Z' / kΩ
DGE
DGE/Apt2
DGE/Apt2/AuNPs-Apt1
DGE/Apt2/AuNPs-Apt1/AuNPs-Apt2
DGE/Apt2/AuNPs-Apt1-DENV-NS1/AuNPs-Apt2
(B)
I / mA
E / V vs Ag/AgCl
DGE/Apt2/AuNPs-Apt1/AuNPs-Apt2
DGE/Apt2/AuNPs-Apt1
DGE/Apt2
(C)
I delta / μA
E step / V vs Ag/AgCl
DGE
DGE/Apt2
DGE/Apt2/AuNPs-Apt1
DGE/Apt2/AuNPs-Apt1/AuNPs-Apt2
(D)
I delta / μA
E step/V vs Ag/AgCl
DGE/Apt2
DGE/Apt2/AuNPs-Apt1
DGE/Apt2/AuNPs-Apt1/AuNPs-Apt2

Fig. 4

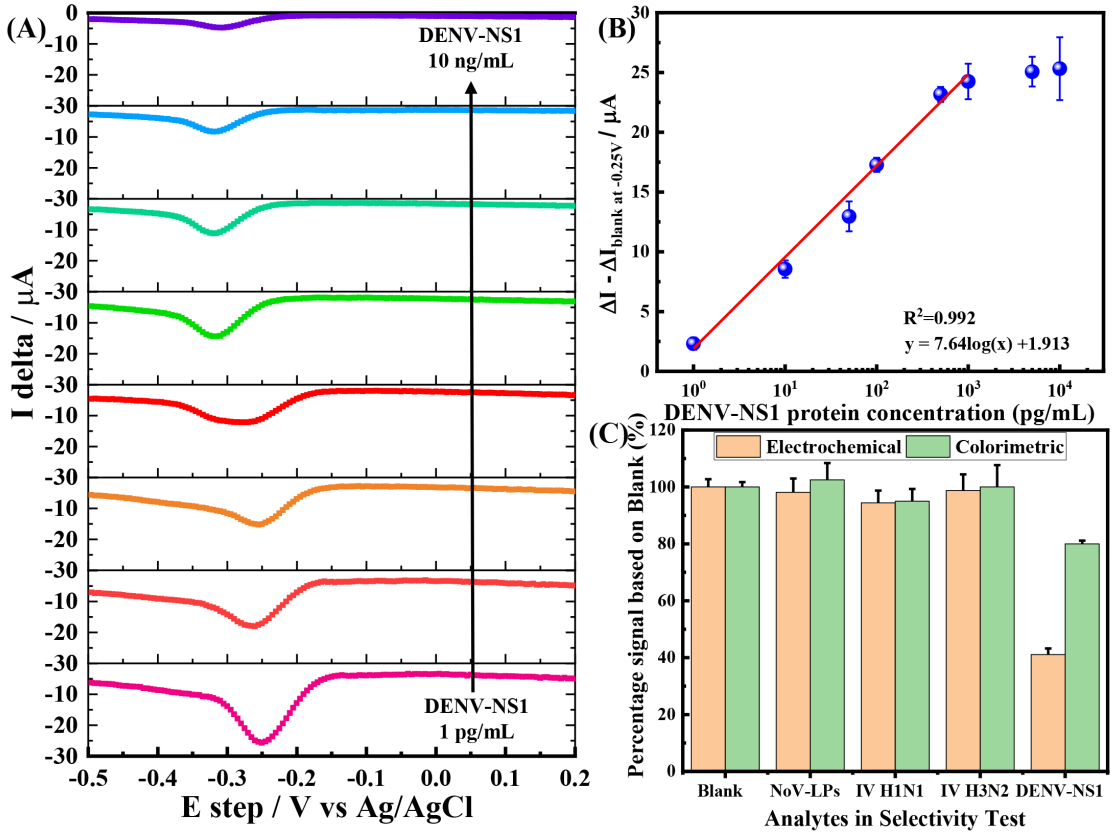
(A)
DENV-NS1
10 ng/mL
DENV-NS1
1 pg/mL
I delta / µA
E step / V vs Ag/AgCl
(B)
ΔI - ΔI blank at -0.25V / µA
R²=0.992
y = 7.64log(x) +1.913
DENV-NS1 protein concentration (pg/mL)
(C)
Electrochemical
Colorimetric
Percentage signal based on Blank (%)
Blank
NoV-LPs
IV H1N1
IV H3N2
DENV-NS1
Analytes in Selectivity Test

Supplementary data

Advancement of dengue virus NS1 protein detection by 3D-nanoassembly complex gold nanoparticles utilizing competitive sandwich aptamer on disposable electrode

Indra Memdi Khoris,[1] Fahmida Nasrin,[2] Ankan Dutta Chowdhury,[2,†] Enoch Y. Park[1,2,*]

[1]Department of Bioscience, Graduate School of Science and Technology, Shizuoka University, 836 Ohya Suruga-ku, Shizuoka 422-8529, Japan

[2]Research Institute of Green Science and Technology, Shizuoka University, 836 Ohya Suruga-ku, Shizuoka 422-8529, Japan

E-mail addresses:
Indra.memdi.khoris.17@shizuoka.ac.jp (IMK)
Fahmida.Nasrin.17@shizuoka.ac.jp (FM)
dc_ankan@yahoo.co.in (ADC)
park.enoch@shizuoka.ac.jp (EYP)

[*] Corresponding author at: Research Institute of Green Science and Technology, Shizuoka University, 836 Ohya, Suruga-ku, Shizuoka 422-8529, Japan.
E-mail address: park.enoch@shizuoka.ac.jp (E.Y. Park). Tel (Fax): +81-54-238-4887)
[†] Current address: Amity Institute of Nanotechnology, Amity University Kolkata, Major Arterial Road (South-East), AA II, West Bengal 700135, India

SI-1 Material and Instruments

SI-1.1. Materials

Two kinds of gold nanoparticles (AuNPs) (5 nm and 20 nm) were obtained from Sigma-Aldrich (St. Louis, MO, USA). Disposable gold electrode (DGE) was purchased from Metrohm Dropsens (C220-BT, Herisau, Switzerland). Streptavidin was obtained from Wako Pure Chemical (Tokyo, Japan). Anti-dengue type 2 NS1 protein aptamer (Apt_1) (Sequence name: ATW0005-BY5-100) and its complementary aptamer (Apt_2) were purchased from Pair Biotechnologies, Inc. (TX, USA). Apt_1 and Apt_2 have a length of 32 nucleotides and 14 nucleotides, respectively. Apt_2 was custom ordered with 3 mismatches evenly spaced over the 14 base lengths.

Influenza virus A and its subtypes were obtained from ProSpec-Tany Technogene, Ltd. (East Brunswick, NJ, USA). Recombinant dengue virus 2 NS1 protein (ab181966) was purchased from Abcam (Cambridge, UK), and 293T whole cell lysate was obtained from Genetex (CA, USA). According to our previous work, norovirus-like particles (NoV-LPs) were prepared from a silkworm expression system [1]. All experiments were conducted using deionized (DI) and autoclaved water.

SI-1.2. Instruments

The absorbance was measured using a clear transparent cuvette (l = 10 mm) by UV-vis spectrophotometer (Shimadzu, Kyoto, Japan) and by using a transparent 96-wells microplate reader (INFINITE 200 M Plex, TECAN, Kanagawa, Japan). Transmission electron microscopy (TEM) images were generated using TEM (JEM-2100F, JEOL, Ltd., Tokyo, Japan) operated at 100 kV. The electrochemical measurement was conducted using Bio-Logic SP-200 Potentiostat and EC-Lab V11.02 software (Bio-Logic Sci. Instruments, Seyssinet-Pariset, France).

SI-1.3. Preparation of Apt_1- and Apt_2-conjugated AuNPs

The conjugation of the aptamers to AuNPs is based on the general streptavidin-biotin binding [2] for anti-dengue type 2 NS1 protein aptamer (Apt_1) forming AuNPs-Apt_1. Initially, 2 mL of AuNPs (0.5 a.u) was mixed with 50 µL streptavidin solution (1 mg/mL) and was incubated for 2 h. Then, the solution containing non-conjugated streptavidin was removed. AuNPs-streptavidin was redispersed in phosphate-buffered saline (PBS) buffer containing 1 mM $MgCl_2$. Apt_1 with biotin on its 5'-end was prior resuspended and refolded according to the instructed protocol from the provider. After refolding, 5 µM of Apt_1 was added to the AuNPs-streptavidin and incubated for 2 h at room temperature. Afterward, the AuNPs-Apt_1 solution was centrifuged to remove excess aptamer. The Apt_1-conjugated AuNPs (AuNPs-Apt_1) were redispersed in PBS buffer containing 1 mM $MgCl_2$.

The conjugation of AuNPs-Apt_2 uses a thiol-Au affinity reaction with Apt_2 aptamer having thiol-group at its 5'-end [3]. The conjugation was simply done by mixing AuNPs (2 mL, 0.5 a.u) and the Apt_1's complementary aptamer (Apt_2) (5 µM), and was incubated for 2 h at room temperature. Afterward, AuNPs-Apt_2 was redispersed in PBS buffer containing 1 mM $MgCl_2$. According to the provider's protocol, the Apt_2 was priorly resuspended, refolded, and reduced.

Table S1. Comparative study of the previous work related to DENV NS1 detection–

Detection Principle	Conjugate	C_{LOD} (ng/mL)	Linear range (ng/mL)	Reference
Immunofluorescence	Antibody	15	15–500	[4]
Electrochemical (EIS[1], SPCE[2])	Antibody	0.3	1–200	[5]
Electrochemical (Capacitive)	Antibody	0.34	1–5000	[6]
Electrochemical (EIS)	Aptamer	0.05	0.01–1000	[7]
Colorimetric	ELISA kit[3]	1	1–100	[8]
Colorimetric	ELISA kit[4]	1.5×10^{-2}	–	[9]
Colorimetric	Aptamer	1.28×10^{-3}	1 – 1000	This work
Electrochemical (DPV)	Aptamer	3.0×10^{-5}	0.001–1	This work

[1]EIS = Electrochemical Impedance Spectroscopy
[2]SPCE = Screen-Printed Carbon Electrode
[3]TANAKA Kikinzoku Kogyo (TKK) ELISA kit
[4]J. Mitra & Co. Pvt. Ltd Dengue NS1 Ag Microlisa kit in dried DENV vector (mosquito)

Table S2. The recovery test of the dual-approach of DENV-NS1 in human serum using AuNPs-Apt$_1$/AuNPs-Apt$_2$ based aptasensor

Sample No.[1]	DENV-NS1 concentration (pg/mL)	Recovery of DENV-NS1 concentration (%)			
		CL.D[2]	RSD[3] (%)	EC.D[4]	RSD (%)
1	2500	98.6	8.50	99.4	10.20
2	1000	112.5	6.15	120.5	8.71
3	500	115.4	4.12	105.1	6.70

[1]DENV-NS1 were spiked in 2% human serum with three independent detections for each sample.
[2]CL.D: colorimetric detection
[3]EC.D: electrochemical detection.
[4]RSD: relative standard deviation calculated from three samples detection.

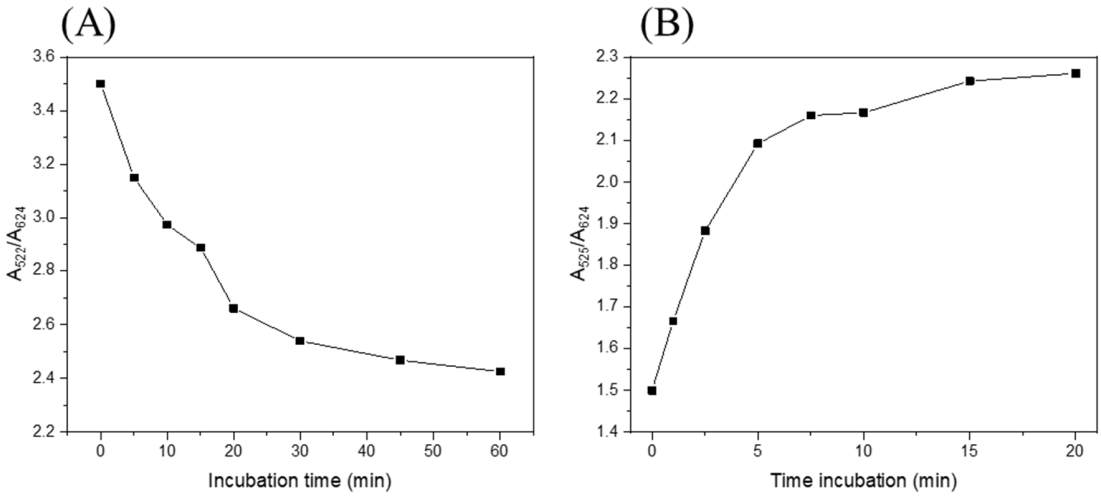

Fig. S1. Optimization of AuNPs-Apt$_1$ and AuNPs-Apt$_2$ binding

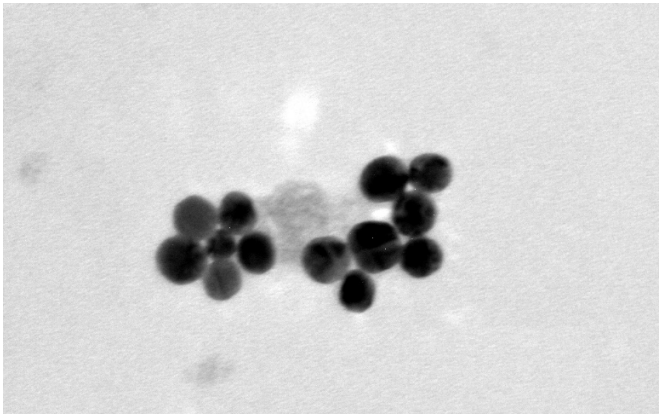

Fig. S2. TEM image of AuNPs/Apt$_1$-NS1/AuNPs-Apt$_2$

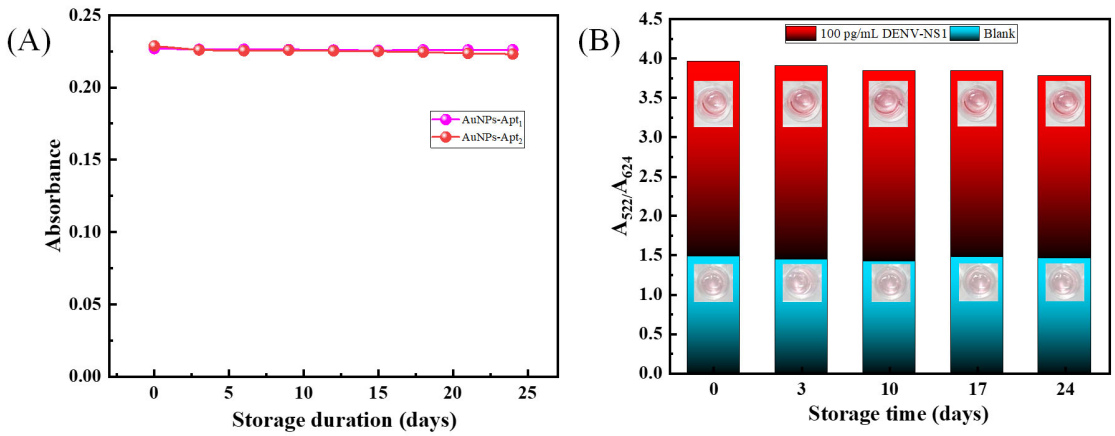

Fig. S3. (A) the absorbance A_{532} of AuNPs-Apt solution in a function of storage duration and (B) performance assessment of AuNPs-Apt during 24-day post-synthesis time.

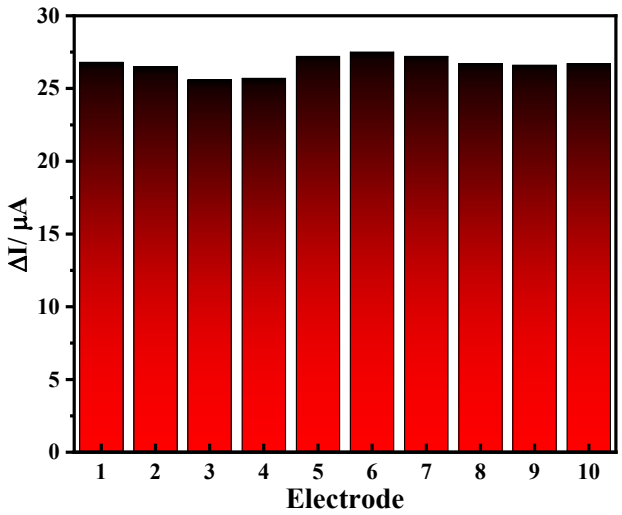

Fig. S4. Reproducibility of the electrochemical baseline signal in 10 electrodes in DPV analysis.

References

[1] J. Boonyakida, D.I.S. Utomo, F.N. Soma, E.Y. Park, Two-step purification of tag-free norovirus-like particles from silkworm larvae (Bombyx mori), Protein Expression Purif., 190 (2022) 106010.

[2] R. Hu, W. Wen, Q. Wang, H. Xiong, X. Zhang, H. Gu, et al., Novel electrochemical aptamer biosensor based on an enzyme–gold nanoparticle dual label for the ultrasensitive detection of epithelial tumour marker MUC1, Biosens. Bioelectron., 53 (2014) 384–389.

[3] S. Giorgi-Coll, M.J. Marín, O. Sule, P.J. Hutchinson, K.L. Carpenter, Aptamer-modified gold nanoparticles for rapid aggregation-based detection of inflammation: an optical assay for interleukin-6, Microchim. Acta, 187 (2020) 13.

[4] N.T. Darwish, S.D. Sekaran, Y. Alias, S.M. Khor, Immunofluorescence–based biosensor for the determination of dengue virus NS1 in clinical samples, J. Pharm. Biomed. Anal., 149 (2018) 591–602.

[5] M.H. Nawaz, A. Hayat, G. Catanante, U. Latif, J.L. Marty, Development of a portable and disposable NS1 based electrochemical immunosensor for early diagnosis of dengue virus, Anal. Chim. Acta, 1026 (2018) 1–7.

[6] A. Santos, P.R. Bueno, J.J. Davis, A dual marker label free electrochemical assay for Flavivirus dengue diagnosis, Biosens. Bioelectron., 100 (2018) 519–525.

[7] B.B. Junior, M.R. Batistuti, A.S. Pereira, E.M. de Sousa Russo, M. Mulato, Electrochemical aptasensor for NS1 detection: Towards a fast dengue biosensor, Talanta, 233 (2021) 122527.

[8] K. Suzuki, E.E. Nakayama, A. Saito, A. Egawa, T. Sato, J. Phadungsombat, et al., Evaluation of novel rapid detection kits for dengue virus NS1 antigen in Dhaka, Bangladesh, in 2017, Virol. J., 16 (2019) 102.

[9] P.R. Abraham, R. Bharathy, P. Kumar, A. Kumar, Dengue NS1 antigen kit shows high sensitivity for detection of recombinant dengue virus-2 NS1 antigen spiked with Aedes aegypti mosquitoes, Sci. Rep., 11 (2021) 23699